Molecular Pharmacology Fast Forward. Published on August 8, 2012 as doi:10.1124/mol.112.080630

A second extracellular site is required for norepinephrine transport by the human norepinephrine transporter

Ching-I A. Wang, Nausad H. Shaikh, Soumya Ramu, and Richard J. Lewis

Institute for Molecular Bioscience, The University of Queensland, St. Lucia, Brisbane, QLD 4072, Australia

Molecular Pharmacology Fast Forward. Published on August 8, 2012 as DOI: 10.1124/mol.112.080630
This article has not been copyedited and formatted. The final version may differ from this version.

Running title page

Running title: Norepinephrine transport mechanism

Address correspondence to: Prof. Richard J. Lewis, Institute for Molecular Bioscience, The University of Queensland, 306 Carmody Road, St. Lucia, Brisbane, QLD 4072, Australia. Tel. 61 7 3346 2984; Fax. 61 7 3346 2101, Email: r.lewis@imb.uq.edu.au

Text: 5916 words

Tables: 2

Figures: 6

References: 66

Text: 17 pages

Abstract: 202 words

Introduction: (991 words)

Discussion: (1689 words)

Abbreviations: *Aquifex aeolicus* leucine transporter ($LeuT_{Aa}$), dopamine (DA), norepinephrine (NE) and serotonin (5-HT), norepinephrine transporter (NET), norepinephrine substrate site (NESS), neurotransmitter sodium symporters (NSS), nisoxetine (NX), selective serotonin reuptake inhibitor (SSRI) structure-activity relationship (SAR), tricyclic antidepressant (TCA)

Molecular Pharmacology Fast Forward. Published on August 8, 2012 as DOI: 10.1124/mol.112.080630
This article has not been copyedited and formatted. The final version may differ from this version.

Abstract

The human norepinephrine transporter (NET) is implicated in many neurological disorders and is a target of tricyclic antidepressants and nisoxetine (NX). We used molecular docking simulations to guide the identification of residues likely to affect substrate transport and ligand interactions at NET. Mutations to alanine identified a hydrophobic pocket in the extracellular cavity of NET, comprising residues W80, F317 and Y467, which was critical for efficient NE transport. This secondary NE substrate site (NESS-2) overlapped the NX binding site, comprising Y84, F317 and Y467, and was positioned ~11 Å extracellular to the primary site for NE (NESS-1). W80 in NESS-2 appeared critical in positioning NE for efficient translocation to NESS-1. Three residues identified to be involved in gating the reverse transport of NE (R81, Q314, D473) did not affect NE affinity for NESS-1. Mutating residues adjacent to NESS-2 abolished NET expression (D75A, L76A) or appeared to affect NET folding (S419A), suggesting important roles in stabilising NET structure, while W308A and F388A at top of NESS-2 abolished both NE transport and NX binding. Our findings are consistent with a multi-step model of substrate transport by NET where a second, shallow extracellular NE substrate site (NESS-2) is required for efficient NE transport by NET.

Molecular Pharmacology Fast Forward. Published on August 8, 2012 as DOI: 10.1124/mol.112.080630
This article has not been copyedited and formatted. The final version may differ from this version.

Introduction

Intracellular communication between neurons in the central nervous system is critically dependent on the controlled release of neurotransmitters at synapses. Monoamine transporters are members of SLC6 family of neurotransmitter sodium symporters (NSS) that use the Na^+ and Cl^- electrochemical gradient to actively remove (transport) biogenic monoamines, including dopamine (DA), norepinephrine (NE) and serotonin (5-HT), from the synapse cleft and back into the nerve terminal (Chen et al., 2004; Masson et al., 1999). Consistent with their crucial role in regulating the strength and duration of synaptic transmission, malfunction or altered expression levels of monoamine transporters are implicated in a number of psychiatric and neurological disorders, including Parkinson's disease (Kim et al., 1997), Wilson disease (Jeon et al., 1998), Lesch-Nyhan disease (Wong et al., 1996), attention deficit hyperactivity disorder (Dougherty et al., 1999), and major depression (Klimek et al., 1997). Moreover, monoamine transporters have been shown to be a primary target for the psycho-stimulants cocaine (Ritz et al., 1987) and amphetamine (Amara and Sonders, 1998), as well as tricyclic antidepressants (TCAs) and analgesic venom peptides (Brust et al., 2009; Nielsen et al., 2005; Sharpe et al., 2001).

Extensive pharmacological and biochemical studies, in conjunction with three-dimensional comparative modelling, have helped characterize the substrate permeation pathway of monoamine transporters and the structural features contributing to substrate and ligand selectivity. However, only since the structure of a related bacterial (*Aquifex aeolicus*) leucine transporter ($LeuT_{Aa}$) was solved (Yamashita et al., 2005) has it been possible to start to develop a detailed molecular view of these interactions. The $LeuT_{Aa}$ crystal structures in complex with substrate leucine (Yamashita et al., 2005) revealed that one leucine and two Na^+ ions were buried in an occluded conformation that was proposed to be a transition state between the open-to-out (substrate binding) and open-to-in (substrate releasing) conformations of the alternating access model of transport (Krishnamurthy et al., 2009). The determination of three $LeuT_{Aa}$-TCA co-

Molecular Pharmacology Fast Forward. Published on August 8, 2012 as DOI: 10.1124/mol.112.080630
This article has not been copyedited and formatted. The final version may differ from this version.

crystal structures (Singh et al., 2007; Zhou et al., 2007) and three $LeuT_{Aa}$-SSRI (selective serotonin reuptake inhibitor) structures (Zhou et al., 2009) revealed an extracellular antagonist binding site S2, ~11Å above the leucine binding site S1, consistent with non-competitive inhibition of leucine by TCAs in $LeuT_{Aa}$ (Singh et al., 2007). More recently, Krishnamurthy and Gouaux successfully trapped $LeuT_{Aa}$ in substrate-free "open-to-out" and "open-to-in" conformations using conformation-specific antibody fragments (Krishnamurthy and Gouaux, 2012). Together with the substrate-bound conformation (Yamashita et al., 2005), this work has defined the structural basis for the alternating access mechanism of NSS symporter transporter.

In separate studies, the Javitch group have identified a second high affinity substrate binding site in $LeuT_{Aa}$ at the position overlapping the S2 site, using steered molecular dynamics in combination with single amino acid imaging (alanine) (Zhao et al., 2011), radiotracer binding and flux experiments (Shi et al., 2008), and equilibrium dialysis with S1- and S2- impaired $LeuT_{Aa}$ mutants (Quick et al., 2012). In these studies, a 2:1 stoichiometry between lecuine and $LeuT_{Aa}$ is observed and both the S1 and S2 sites can be occupied simultaneously. Javitch group further demonstrated the pivotal involvement of the S2 site in substrate transport by introducing mutations at S2 (Shi et al., 2008) or blocking S2 with TCA (Shi et al., 2008) and commonly used crystallisation detergent octylglucoside (Quick et al., 2009), seen in $LeuT_{Aa}$ crystal structures (Singh et al., 2008; Singh et al., 2007). Based on these data, this group has proposed a modified hypothesis where the alternating access mechanism is initiated when a second leucine binds to S2 and triggers a conformational change to open-to-in, allowing release of a lecuine already bound to S1. Despite considerable effort to resolve this point of difference (Piscitelli et al., 2010; Quick et al., 2012; Wang et al., 2012), the requirement for a second substrate site for NSS symporter function remains in debate.

In addition to helping elucidate the mechanisms of substrate transport, $LeuT_{Aa}$ shares many structural and functional similarities to related monoamine transporters allowing predictive

Molecular Pharmacology Fast Forward. Published on August 8, 2012 as DOI: 10.1124/mol.112.080630
This article has not been copyedited and formatted. The final version may differ from this version.

homology models to be constructed (Andersen et al., 2009; Beuming et al., 2008; Beuming et al., 2006; Erreger et al., 2008; Forrest et al., 2007; Forrest et al., 2008; Huang and Zhan, 2007; Indarte et al., 2008; Jacobs et al., 2007; Mitchell et al., 2004; Norregaard et al., 1998; Rudnick and Wall, 1992; Smicun et al., 1999; Stephan et al., 1997; Tavoulari et al., 2009; Zhang and Rudnick, 2006; Zhou et al., 2007; Zhou et al., 2009; Zomot et al., 2007). For example, homology models built from $LeuT_{Aa}$ have been used to identify putative Cl^- binding sites in serotonin (SERT), dopamine (DAT) and GABA (GAT-1 and -4) transporters (Forrest et al., 2007; Zomot et al., 2007) that predict Cl^- ions regulate the equilibrium between the open-to-out (substrate binding) and open-to-in (transporting) states (Beuming et al., 2008; Erreger et al., 2008; Forrest et al., 2008; Tavoulari et al., 2009). Homology models have also identified a conserved substrate binding site, equivalent to the leucine site identified in $LeuT_{Aa}$-Leu (Yamashita et al., 2005), which is present across norepinephrine (NET), glycine (GlyT), tryptophan (TnaT) and tyrosine (Tyt1) transporters (Beuming et al., 2006; Paczkowski et al., 2007).

Here, we used a combination of homology modelling, molecular docking simulations, and site-directed mutagenesis to identify residues affecting NE transport and the binding of its competitive inhibitor nisoxetine (NX, a selective norepinephrine reuptake inhibitor (SNRI) (Jayanthi et al., 1993)) in the extracellular mouth of human NET. The NX binding site was found to overlap with the S2 binding site for SSRIs (Zhou et al., 2009) and TCAs (Singh et al., 2007) co-crystallized with $LeuT_{Aa}$, whereas two NE binding sites critical for efficient substrate transport were identified. The apparent high affinity site for NE (NESS-1) overlapped the leucine binding site (S1) identified in $LeuT_{Aa}$-Leu (Yamashita et al., 005), while a lower affinity site for NE (NESS-2) was identified ~ 11 Å extracellular to NESS-1. The predicted residues contributing to NE and NX transport and binding were confirmed by site-directed mutagenesis. Our findings support a multi-step model of substrate transport by NET.

Molecular Pharmacology Fast Forward. Published on August 8, 2012 as DOI: 10.1124/mol.112.080630
This article has not been copyedited and formatted. The final version may differ from this version.

Materials and Methods

Molecular Modelling and Docking. A molecular model of NET was built using the $LeuT_{Aa}$-Leu (PDB ID 2A65 (Yamashita et al., 2005)) co-crystal structure as the template with the program *Modeller 9v2* (Fiser and Sali, 2003). All sequence alignments were generated using *ClustalW* (Larkin et al., 2007) and were corrected manually based on the secondary structure analysis using *Phyre* (Kelley and Sternberg, 2009) and TMHMM (Krogh et al., 2001) to guide the sequence alignment of the TMHs and low homology regions, especially for ELs (Supplemental Figure 1). Similar sequence alignment approaches have successfully revealed residues in SLC6 transporters that are likely to regulate substrate binding selectivity and transport mechanism (Beuming et al., 2006). All resulting homology models were subjected for energy minimization using GROMOS 96 (Gunsteren and Berendsen, 1990) with 500 steps of steepest descent followed by 1,000 cycles of conjugated gradient, to remove steric incompatibilities. The structural models were evaluated using the online server *Verify3D* (Bowie et al., 1991) and Ramachandran plot available from *ProFunc* (Laskowski et al., 2005) database. The few residues with unfavourable geometry were relaxed by manually selecting the backbone and side chain atoms with consecutive energy minimization using GROMOS 96 or by rigid body refinement using Coot (Emsley and Cowtan, 2004) until the geometry was satisfactory. Assessment of the structure of the NET homology model relative to $LeuT_{Aa}$ (PDB ID 2A65) using the relationship between the protein sequence identity and expected model accuracy (Forrest et al., 2006) supported the sequence alignment (Supplemental Figure 1) and resulting quality of the NET model generated (Table 1).

We presumed that there would be little conformational change between the substrate-bound and inhibitor-bound states based on the crystallographic parameter b-factors and 3D superimposition of co-crystal structures of $LeuT_{Aa}$ with substrate (Leu) (Yamashita et al., 2005), amino acids (Ala, Gly, Met, Phe) (Singh et al., 2008), SSRIs (setraline, *R*-fluoxetine, *S*-fluoxetine) (Zhou et al., 2009) and TCAs (desipramine, imipramine, clomipramine) (Singh et al., 2007; Zhou et al., 2007).

Molecular Pharmacology Fast Forward. Published on August 8, 2012 as DOI: 10.1124/mol.112.080630
This article has not been copyedited and formatted. The final version may differ from this version.

Therefore, rigid-docking simulation was chosen for searching possible NE and NX binding sites in NET to avoid approach-dependent bias. Structures of NE (Drug Bank database) and its competitive inhibitor NX (generated using program *CORINA* (Accelrys)) were docked to the NET homology models, including NET and W80A-NET, with three-dimensional fast Fourier transformation docking approaches with high order (*N*=25) spherical polar Fourier correlation followed by Newton-like energy minimization using the program *HEX 5.0* (Ritchie and Kemp, 2000).

Solutions with spatially similar docking orientation (RMSD < 3Å) were grouped and the lowest energy solution from each group was chosen as a candidate for further analysis. Semi-flexible docking simulations using *Autodock Vina* (Trott and Olson, 2010) was then performed to optimise the intermolecular interactions, where both ligands and side chains of the binding site residues predicted by *HEX 5.0* were set to be rotatable. The centre of the grid map was set as the centre of ligands with dimensions of 20 x 20 x 20 Å, covering the predicted binding site, with a searching resolution of 1 Å. The 10 lowest energy solutions for NX and NE docked to NESS-2 of hNET had minimal energies within 5 kcal/mol (Supplemental Figure 2). All ten docking solutions for NE and NX were similar (RMSD 1.5 and 1.7 Å, respectively) but non-identical, with the lowest energy docking solution chosen for detailed analysis. Hydrogen bonds between ligands and NET that are likely to contribute to substrate and inhibitor binding were analyzed using the online server *WHAT IF* (Vriend, 1990). To determine the influence of mutations on substrate and inhibitor binding, we mutated residues D75, R81, W308, Q314, F316, S419 that were found to form intra-molecular interactions in a close proximity to the predicted substrate binding site in the homology models. A NET model derived from the $LeuT_{Aa}$-Trp co-crystal structure failed to dock NE using *HEX 5.0*.

NET mutants. Site-direct mutagenesis of human NET was performed as previously described (Paczkowski et al., 2007) using custom made primers and the QuickChange kit (Stratagene, La

Molecular Pharmacology Fast Forward. Published on August 8, 2012 as DOI: 10.1124/mol.112.080630
This article has not been copyedited and formatted. The final version may differ from this version.

Jolla, CA). All mutants were sequenced to verify each mutation. Plasmids of interest were transformed into TOP-10 competent *Escherichia coli* cells (Invitrogen) for large scale DNA purification and storage prior to transfection.

(^{3}H)Norepinephrine uptake assays. COS-7 cell (ATCC, Manassas, VA) were cultured in Dulbecco's modified Eagle's medium (DMEM) containing 10% fetal bovine serum (FBS) in 96-well plates. At ~ 90% confluence, cells were transiently transfected with NET and NET mutant cDNA using 10 μl FuGENE (Roche, Australia) and 2 μg DNA per 10^6 cells. Twenty-four hours post-transfection, 10,000 cells were aliquoted per well in a 96-well plate format for additional 24 h incubation to obtain a count of ~ 50,000 cells per well prior to initiation of the uptake assays. Substrate transport efficiency was determined with increasing concentrations of (^{3}H)norepinephrine ((^{3}H)NE; 40.5 Ci/mmol, Perkin Elmer) from 10^{-8} M to 5 x 10^{-6} M in a final volume of 50 μl in 96-well plates and incubated at 37 °C for 10 min, followed by two gentle washes using 100 μl assay buffer (25 mM HEPES, pH 7.4, 125 mM NaCl, 1.2 mM $MgSO_4$, 4.8 mM KCl, 1.2 mM KH_2PO_4, 1.3 mM $CaCl_2$, 5.55 mM D-(+)-glucose, 1 mM ascorbic acid) to remove excess (^{3}H)NE. Non-specific uptake of (^{3}H)NE by transfected cells was determined in the presence of 200 μM NX. After incubation, cells were lysed using 50 μl of 0.1 M NaOH with gentle shaking for 60 min. The specific (^{3}H)NE uptake was calculated as the difference between the total cellular uptake and the non-specific uptake. Each experiment was performed in triplicate in at least three separate experiments.

(^{3}H)Nisoxetine binding assays. Human NET transfected (see above) COS-7 cell membrane was used to measuring (^{3}H)NX (81.7 Ci/mmol, Perkin Elmer) binding to NET. Transfected cells were washed and scraped off in the assay buffer containing 1.6 mg/ml protease inhibitor cocktail (Roche Diagnostics, USA), followed by sonication at 4 ºC for 25 seconds. Cell debris was subsequently removed by centrifugation at 465 × *g* for 10 min and the membrane pelleted at 39,000 × *g* for 30 min at 4 ºC, and finally resuspended in assay buffer. Assays containing 20 μg of

Molecular Pharmacology Fast Forward. Published on August 8, 2012 as DOI: 10.1124/mol.112.080630
This article has not been copyedited and formatted. The final version may differ from this version.

total membrane protein per concentration (Bradford assay, Bio-rad) and increasing concentrations of (^{3}H)NX from 10^{-10} M to 5 x 10^{-8} M in a final volume of 50 µl were incubated in 96-well plates on ice for 60 min. After incubation, membrane was filtered onto a Filtermat B and washed twice with cold assay buffer to remove unbound (^{3}H)NX using a Filtermat-96 Harvester (Perkin Elmer). Filtermats were dried in the incubator at 37 ºC overnight, placed in Topseal-A 96 well sleeve (Perkin Elmer) with Betaplate scintillant (Perkin Elmer) and sealed prior to measurement of radioactivity in a Microbeta counter (Perkin Elmer). Non-specific binding of (^{3}H)NX was determined in the presence of 200 µM NX and specific (^{3}H)NX binding calculated as the difference between the total cellular and the non-specific binding. Each experiment was performed in triplicate and repeated four or five times.

Inhibition of (^{3}H)nisoxetine binding by norepinephrine. NE binding affinity was determined from the displacement of (^{3}H)NX from human NET mutants W80A, R81Q, Y84A, L160A, F164A, Q314A, F316A, Y467F, D473A, D473R and R81D/D473R, which showed no NE uptake and yet retain NX binding function in uptake and binding single-point and saturation assays. The assays were performed as described in (^{3}H)NX binding assays using a fixed concentration of (^{3}H)NX of 3 nM and increasing concentrations of NE from 10^{-14} M to 10^{-3} M in 10-fold increments. Each experiment was performed in triplicate and repeated three times.

Inhibition of (^{3}H)norepinephrine transport by nisoxetine. NX affinity was determined from the inhibition of (^{3}H)NE binding to the mutant Y84A-NET to determine the impacts of mutations on NX binding ability. Assays were conducted for mutants L160A and F164A as they showed comparable NX binding (K_D) to wild type NET to support the hypothesis of only one NX binding site in NET. The assays were performed as described in (^{3}H)NE uptake assays using a fixed concentration of (^{3}H)NE of 30 nM and increasing concentrations of NX from 10^{-14} M to 10^{-3} M in 10-fold increments. Each experiment was performed in triplicate and repeated three times.

Molecular Pharmacology Fast Forward. Published on August 8, 2012 as DOI: 10.1124/mol.112.080630
This article has not been copyedited and formatted. The final version may differ from this version.

Western blot. Western blots were prepared for determining the total expression using 20 μl cell membrane (20 μg of total protein) prepared as described for (^{3}H)NX binding assays, mixed with 5 μl SDS (sodium dodecyl sulfate) loading dye (0.225 M Tris-HCl, pH 6.8; 50% (v/v) glycerol, 5% (w/v) SDS, 0.05% (w/v) bromophenol blue; 500 mM β-mercaptoethanol) and incubated at room temperature for 10 min before SDS-polyacrylamide gel electrophoresis (SDS-PAGE). 4–12 % NuPAGE gels (Invitrogen) were utilized to separate the native and mutated NET proteins from other cellular proteins. Following electrophoresis, proteins of interests were transferred to nitrocellulose membrane (BioRad). After the transfer, the membranes were blocked in blocking solution (5 % (w/v) skim milk) for one hr, followed by 45 min incubation with sequence-specific antibody (1:3000 enzyme to blocking solution ratio; mouse monoclonal antibody to NET (targeting N-terminal amino residues 17–33, AbCam, USA). After incubation, the membrane was washed (3 × 5 min) in blocking solution to remove excess primary antibody before the secondary antibody (fluorescently-labelled goat anti-mouse igG (H+L) Alexa Fluor 680, Molecular Probes) was added (1:2500 enzyme to blocking solution ratio) and allowed to bind for a further 45 min. Finally, the membranes were washed (3 × 1 min) in a large volume of phosphate buffer solution and scanned using the *Odyssey IR imaging system* (LI-COR Biosciences). As is the case for most membrane proteins, they generally migrate faster in SDS-PAGE as an artefact of SDS-lipid micelle complex. The molecular weight of NET wild type in total expression is observed as ~ 54 kDa in SDS-PAGE that corresponds to the literature (Hahn et al., 2003).

Results

Identification of residues in NESS-2 with direct or local effects on NE transport and NX affinity. To identify potential direct interacting residues, we docked NE and NX onto a homology model of NET generated using the $LeuT_{Aa}$-leu (Yamashita et al., 2005) co-crystal structure as the template. Docking simulations revealed two potential norepinephrine substrate binding sites on

Molecular Pharmacology Fast Forward. Published on August 8, 2012 as DOI: 10.1124/mol.112.080630
This article has not been copyedited and formatted. The final version may differ from this version.

NET, we named NESS-1 and NESS-2, as well as a single binding site for NX that overlapped NESS-2. NX was found to occupy a similar binding pocket to that observed previously for TCAs co-crytallised with $LeuT_{Aa}$ (Fig. 1) (Singh et al., 2007), while the ~ 11 Å deeper NESS-1 overlapped the S1 site identified for $LeuT_{Aa}$-leu co-crystal structure by (Yamashita et al., 2005) (Fig 1*A*).

Analysis of NE and NX docking results revealed that residues F317 (TMH6a) and Y467 (TMH10) might contribute to both NX and NE binding, L76 and W80 (TMH1b) might be NE specific, whereas Y84 (TMH1b) was likely to be NX specific (Fig. 1*A* and 1*C*). The direct intermolecular interactions observed to coordinate NE at NESS-2 included a hydrogen bond between the β-hydroxyl of NE and the tyrosine hydroxyl (Y467) at a distance of 2.3 Å, a T-stacking π interaction between the two benzene rings of NE and Y467, and a cation-π interaction between the positively charged catecholamine of NE and benzene ring of F317 at a distance of 2.0 Å (Fig. 1*B*). L76 and W80 were predicted to provide additional hydrophobic and van-der-Waals interactions to coordinate NE binding at distances of 3.2 and 3.8 Å, respectively (Fig. 1*B*).

Like NE, NX binding was dominated by hydrophobic interactions, where the methoxy-benzene of NX formed a π-π interaction with Y467 (~ 3.1 Å), and the benzene ring of NX formed a T-stacking π interaction with Y84 (~ 3.8 Å). In addition, our model predicted that the nitrogen on the dimethylbenzylamine of NX formed a cation-π interaction with F317 (~ 3.2 Å), as previously observed for NE (Fig. 1*B*). Further examination of the NET model revealed several hydrophobic residues in the cavity of NET that might indirectly influence NESS-2 residues. F164 on TMH3 appeared to form a T-stacking π interaction with W80 and a strong hydrophobic interaction with L76, suggesting that F164 might influence the side chain orientations of L76 and W80 and indirectly influence their interactions with NE (see above). In addition, L160 (TMH3) together with L76, W80 and F164 form a contiguous hydrophobic patch that could interact directly with the catecholbenezene ring of NE (Fig. 1*B*).

Molecular Pharmacology Fast Forward. Published on August 8, 2012 as DOI: 10.1124/mol.112.080630
This article has not been copyedited and formatted. The final version may differ from this version.

Identification of additional residues predicted to contribute to the structure of NESS-2. A number of residues outside NESS-2 were also identified in this NET model that might be expected to influence the structural integrity of NESS-2. Given their prominent positions, W308 and F316 could act as hydrophobic anchors to stabilise each end of TMH6a, which extends between NESS-2 and NESS-1 (Fig. 2*A* and 2*B*, respectively), to affect the flexibility and integrity of TMH6a, which has previously been proposed to be essential for substrate transport (Yamashita et al., 2005). In NET, W308 is cradled by a hydrophobic patch formed by P97 and L100 on TMH2, L302 on EL3, and F528 on TMH11, whereas F316 forms an extensive hydrophobic network with F101 (T-stacking π) on TMH2, and I481, L482 and V485 on TMH10 (Fig. 2*B*). A second hydrophobic network formed by F388 on EL4 interacting with W80 on TMH1, F167 on TMH3 and F409 on TMH8, was also predicted to contribute structurally to the conformation of NESS-2 (Fig. 2*C*), given that conformational movements of EL4 in $LeuT_{Aa}$ (Singh et al., 2007), GAT-1 (Zomot and Kanner, 2003), DAT (Norregaard et al., 1998), GlyT1b (Ju et al., 2004) and SERT (Mitchell et al., 2004) have been previously demonstrated to accompany substrate and inhibitor binding.

Two residues D75 (TMH1b) and S419 (TMH8) were also identified that might indirectly affect NE transport or NX binding by altering the structural stability of NESS-2 in NET (Fig. 2*D)*. As observed in $LeuT_{Aa}$ crystal structure (Yamashita et al., 2005), the electron density of leucine and both Na^+ ion binding sites are well-defined, with potentially the leucine and Na^+ ions contributing to this structural stabilization. D75 has previously been proposed to substitute for G24 in $LeuT_{Aa}$ and coordinate Na^+ ions (Barker et al., 1999; Beuming et al., 2006; Henry et al., 2006; Huang and Zhan, 2007; Indarte et al., 2008), while S419 contributes to substrate binding in SERT (Andersen et al., 2009). That these residues are fully conserved across monoamine transporters (equivalent to D79 and S421 in DAT; D98 and S438 in SERT), further highlights their potential functional significance. Based on our modelling, we propose that D75 and S419

Molecular Pharmacology Fast Forward. Published on August 8, 2012 as DOI: 10.1124/mol.112.080630
This article has not been copyedited and formatted. The final version may differ from this version.

may contribute to the structural stability of NET via ion and substrate binding, as observed in $LeuT_{Aa}$ (Beuming et al., 2006; Henry et al., 2006; Huang and Zhan, 2007; Indarte et al., 2008) and SERT (Andersen et al., 2009). Therefore mutating D75 or S419 to alanine destabilize NET structure to affect NE transport and/or NX binding.

Identification of residues predicted to gate the reverse transport of NE. A hydrogen bond in $LeuT_{Aa}$ (R30–Q250) is disrupted upon TCA binding, allowing the side chain of R30 to rotate ~ 110º where it can form two salt bridges with D404 (equivalent to D473 in NET) (Singh et al., 2007) that gate the reverse transport of substrate (Chen et al., 2003; Singh et al., 2007; Zhou et al., 2007). Given that R30 and D404 in $LeuT_{Aa}$ are conserved at equivalent positions across all SLC6 transporters, members of the SLC6 family are likely to share a common gating mechanism. This gating mechanism is also likely to affect NX inhibition, since the amine tail of NX is predicted to prevent the formation of these salt bridges as seen in the $LeuT_{Aa}$–TCA co-crystal structures (Singh et al., 2007). To evaluate this gating mechanism in NET, we assessed NE transport and NX binding in the R81A, R81Q, R81D, Q314A, D473A, D473R, R81Q/Q314R, R81A/Q314A, R81D/D473R mutants of NET.

Functional characterization of docking predictions. To experimentally test our docking prediction, we created 22 mutants of NET. All mutants were evaluated by immunodetection, binding and uptake assays to determine the effects on NE transport and NX binding kinetics (Fig. 3 and 4).

Alanine substitutions at four of the five residues in NESS-2 that were predicted to have direct affects on NE and/or NX affinity (W80A, Y84A, F317A, Y467A) had no significant effect on the levels of NET expression determined by immunodetection, while L76A abolished NET expression (Fig. 3*A*). Supporting our predictions, the Y467A and F317A mutants abolished both NE transport and NX binding (Fig. 3*B*). In contrast to Y467A, Y467F-NET reduced NE ability to displace NX by ~ 3.5-fold, without significantly affecting the apparent Michaelis constant K_M

Molecular Pharmacology Fast Forward. Published on August 8, 2012 as DOI: 10.1124/mol.112.080630
This article has not been copyedited and formatted. The final version may differ from this version.

(defined as extracellular NE concentration required for half maximal transport velocity (V_{MAX})) or the NX binding affinity (K_D) (Fig. 4*A* and 4*C*, and Table 2). The Y467F mutant produced a ~ 9-fold reduction in substrate transport efficiency (V_{MAX}) that corresponded to the ~ 6-fold drop in transporter expression determined from the B_{MAX} for ^{3}H-NX (Table 2). Mutant Y84A reduced NX binding affinity by ~ 5-fold, which correlated with a ~ 10-fold reduction in NX inhibition of NE transport (IC_{50}), without significantly affecting K_M or V_{MAX} (Fig. 4, and Table 2). Finally, mutating the predicted NE-specific residue W80 to alanine abolished NE transport (Fig. 4). Interestingly, this mutant retained wild-type affinity for NE to displace ^{3}H-NX binding and significantly enhanced (~ 5-fold) NX affinity (Fig. 4 and Table 2).

F164 and L160 were identified to form part of a contiguous hydrophobic patch in NESS-2, together with W80 and L76. The F164A mutant caused a 5-fold reduction in K_M (Fig. 4*A*), indicating that this hydrophobic network is not optimal for NE transport. This mutant did not influence ^{3}H-NX affinity, and the modest ~ 3-fold reduction in V_{MAX} corresponded to the observed decrease in transporter expression (B_{MAX}) (Fig. 4*B* and Table 2). In contrast, the L160A mutant did not significantly affect any of the measured parameters for NET (Fig. 4 and Table 2), indicating these similar residues are interchangeable.

D75 and S419 were predicted to play critical roles in stabilizing NET structure via interactions with substrate and Na^+ ion at NESS-1, respectively, as observed in $LeuT_{Aa}$ (Yamashita et al., 2005). Immunodetection analysis revealed that D75A almost completely abolished NET expression, whereas S419A appeared to cause misfolding that resulted in a decrease in apparent molecular size of NET (Fig 3*A*). These effects on expression account for the almost complete loss of NE transport and NX binding observed for these mutants (Fig. 3).

Residues contributing to the hydrophobic interactions associated with NESS-2 and NESS-1 were also investigated. W308A and F388A appeared to express normally but failed to show detectable NE uptake or NX binding, while the F316A mutant had significantly impaired

Molecular Pharmacology Fast Forward. Published on August 8, 2012 as DOI: 10.1124/mol.112.080630
This article has not been copyedited and formatted. The final version may differ from this version.

NE transport efficiency (~ 30-fold reduced V_{MAX}) despite NE K_M and IC_{50} to displace ^{3}H-NX remaining unchanged (Table 2; Fig. 3 and 4).

Despite normal expression (Fig 3*A*), all mutations generated at the three proposed extracellular gating residues R81, Q314 and D473 significantly diminished or abolished NE uptake. Q314A retained wild-type affinity for NE to displace ^{3}H-NX, while D473A produced a ~ 6-fold reduction (Fig 3*B* and 4*B*). The R81A, R81D, R81A/R314A and R81Q/Q314R mutants each abolished detectable NE transport and NX binding (Fig. 3B). The R81Q, Q314A, D473A, D473R and R81D/D473R mutants also failed to generate detectable NE transport but all bound ^{3}H-NX, albeit mostly at reduced levels. Interestingly, despite abolishing transport the IC_{50} to displace ^{3}H-NX remained unchanged (Table 2), with four mutants (Q314A, D473A, D473R and R81D/D473R) producing significant (~4-fold) improvements in NX affinity (Fig. 4*C* and Table 2).

Discussion

The molecular docking simulations and mutagenesis data reported in this study are consistent with two substrate sites being required for NE transport by NET. The first NE substrate site (NESS-2) encountered by NE is located close to the extracellular mouth of NET and is maintained by residues lining the TMH1b-3-6a-8-10 bundle. The second NE substrate site (NESS-1) is positioned ~ 11 Å below NESS-2 and overlaps the Leu binding site previously identified in $LeuT_{Aa}$ crystal structure (Yamashita et al., 2005). From analyses of these docking and mutational studies, it appears that NESS-2 might orientate NE for efficient translocation to the deeper site NESS-1. An extracellular substrate binding site has also been identified in SERT and $LeuT_{Aa}$, respectively (Quick et al., 2012; Shi et al., 2008; Zhao et al., 2011; Zhou et al., 2009), suggesting that this feature may be common among SLC6 transporters. Interestingly, the NX binding site in NET was found to partially overlap NESS-2 but not NESS-1 (Fig. 1) at a

Molecular Pharmacology Fast Forward. Published on August 8, 2012 as DOI: 10.1124/mol.112.080630
This article has not been copyedited and formatted. The final version may differ from this version.

location similar to the SSRI and TCA binding site identified in $LeuT_{Aa}$ (Singh et al., 2007; Zhou et al., 2009). Thus the presence of NESS-2 explains the ability of NX and TCAs to competitively inhibit NE transport by NET (Jayanthi et al., 1993).

Of the five hydrophobic residues predicted to directly interact with NE and/or NX, mutating four (L76A-NET failed to express) to alanine abolished NE transport (W80, F317, Y467) or NX binding (Y84, F317, Y467), suggesting that both NE and NX binding are dominated by extensive hydrophobic interactions. The reduced affinity of NX for the Y84A mutant likely arises because the predicted T-stacking π interaction with NX is disrupted. Loss of both NE transport and NX binding for the F317A mutant supports our modelling prediction that these residues directly coordinate NE and NX binding at NESS-2 via a cation-π interaction. The almost complete loss of NE uptake and NX binding at Y467A-NET, but almost full NE and NX affinity at Y467F-NET, supports the prediction that Y467 forms a T-stacking π and hydrogen bond interaction with NE and only a π-π interaction with NX (Fig. 1). The role of L76, predicted to directly interact with NE or binding, could not be tested since the alanine substitution unexpectedly abolished NET expression. Given L76 is the first residue of TMH1b and forms an extensive hydrophobic network with W80, L160 and F164 (Fig. 1*B*), a role in stabilising the structure of NET is proposed in addition to any potential specific role in NE transport or NX binding.

To further understand the pivotal role played by W80 in NE transport, we docked NE at a model of W80A-NET (Fig. 5.). This simulation revealed a significant shift in NE docking to now completely overlap the NX binding site, which was little altered in this new model (Fig. 5). Despite the loss of NE transport observed experimentally, NE maintained a similar affinity to displace (^{3}H)NX from W80A-NET. This result suggests that the loss of the hydrophobic interactions contributed by W80 are compensated by neighbouring hydrophobic residues that reposition NE so that it can no longer be transported. Thus a single amino acid change can

Molecular Pharmacology Fast Forward. Published on August 8, 2012 as DOI: 10.1124/mol.112.080630
This article has not been copyedited and formatted. The final version may differ from this version.

convert NE from a transportable substrate to an antagonist of NX binding to NET. Based on this interpretation, we propose that W80 is required to correctly position NE at NESS-2 for efficient translocation to NESS-1.

In addition to these direct interactions, we identified five positions (D75, W308, F316, F388, S419) that might influence the structure of NESS-2 and -1 (Fig. 2). Consistent with the modelling predictions, mutating these residues to alanine either inhibited NET expression (D75), caused protein truncation (S419), or abolished NE transport and/or NX binding (W308, F316, F388). The inhibited NET expression or truncation seen for the D75A and S419A mutants, respectively, presumably arises from the disruption of coordinating Na^+ ions (Barker et al., 1999; Beuming et al., 2006; Henry et al., 2006; Huang and Zhan, 2007; Indarte et al., 2008; Yamashita et al., 2005). The high degree of conservation of both D75 and S419 in SLC6 transporters suggests that these residues likely play similar structural roles in other SCL6 transporters including SERT (Barker et al., 1999) and $LeuT_{Aa}$ (Yamashita et al., 2005). Residues W308 and F388 (Fig 2) were predicted to contribute to the stabilization of TMH2-6a-10-11 bundle and TMH1b-3-8 and EL4, respectively. W308 is located at end of TMH6a where it could influence the α-helical structure of TMH6a and potentially influence any conformational movement associated with substrate transport. F388 is located in EL4, where it could influence the EL4 flexibility, which was previously found to be important for substrate binding (Ju et al., 2004; Mitchell et al., 2004; Norregaard et al., 1998; Singh et al., 2007; Zomot and Kanner, 2003). Finally, the F316A mutant predicted to also affect the stability of the TMH2-6a-10 bundle, reduced NE transport efficiency to ~ 3% of wild-type, without affecting its K_M or its ability to displace ^{3}H-NX. Reduced NE transport efficiency in the absence of any effect on NESS-2 (NE and NX IC_{50}s unchanged) or NESS-1 (NE K_M unchanged) suggests this mutation may reduce the rate of the transitions between the open-to-out and open-to-in conformations, and implies that the transition to the open-to-in conformation occurs after substrate binds at NESS-1.

Molecular Pharmacology Fast Forward. Published on August 8, 2012 as DOI: 10.1124/mol.112.080630
This article has not been copyedited and formatted. The final version may differ from this version.

Based on an analysis of the $LeuT_{Aa}$ crystal structure (Yamashita et al., 2005), an additional three residues, R81, Q314, and D473 (Fig. 2*D*), were predicted to form an extracellular gate in NET that would restrict reverse transport and facilitate forward transport. Consistent with such a role, mutating R81Q, Q314A, D473R, D473A and R81D/D473R abolished NE uptake with little affect on NX or NE binding affinity. R81A, R81D, R81A/Q314A and R81Q/Q314R mutants of NET abolished both NX binding and NE transport. Loss of NE transport in the Q314A mutant suggests that the hydrogen bond between Q314 and R81 observed in the $LeuT_{Aa}$ crystal structure (Yamashita et al., 2005) is required to restrict formation of a salt bridge between R81 and D473 NE prior to NE binding to NESS-1. Upon NE binding to NESS-1, this H-bond is broken allowing R81 to reorientate to form a salt bridge with D473 to create an extracellular gate. Once formed, this salt bridge is then expected to facilitate structural transitions from the open-to-out to the open-to-in conformation.

K_M and IC_{50} are separate measures of affinity, with the former influenced by transport asymmetry, multiple substrate binding sites, and the multiplicity of conformations in each cycle. However, the large difference between K_M (1 μM) for NE transport and the IC_{50} (59 μM) for NE displacement of NX binding is suggestive of two substrate affinities for NE. This distinct difference was observed across all mutants [Y84A (~ 135-fold), L160A (~ 80-fold), F164A (~ 350-fold), F316A (~ 40-fold), Y467F (~ 350-fold)] that retained the ability to transport NE. Interestingly, the Y467A mutant differentially affected the IC_{50} for NE without affecting its K_M. Based on these results, we propose that the low affinity site determined from NE displacement of NX binding corresponds to NE binding at NESS-2, while the K_M for NE is likely driven through higher affinity interactions at NESS-1. This conclusion is consistent with the previously observed competitive interaction between NX and NE (Jayanthi et al., 1993).

The impacts of mutants W80A, R81Q, Q314A, D473A, D473R, R81D/D473R, which completely abolished substrate transport and yet retained the low affinity binding interaction,

Molecular Pharmacology Fast Forward. Published on August 8, 2012 as DOI: 10.1124/mol.112.080630
This article has not been copyedited and formatted. The final version may differ from this version.

provides experimental support for the presence of two distinct substrate binding sites in NET. The recent studies on $LeuT_{Aa}$ (Quick et al., 2012; Shi et al., 2008; Zhao et al., 2011), hSERT (Sinning et al., 2010) and the carnitine transporter (CaiT) crystal structure (Tang et al., 2010) have also proposed a two-site model for substrate transport.

Taken together, our results support a multi-step model for substrate transport by NET as summarised in the scheme shown in Fig. 6. In this model, NE binds first to a low affinity site at NESS-2 in an substrate binding conformation similar to that observed in the $LeuT_{Aa}$-Leu co-crystal structure (Fig. 6*A*) (Yamashita et al., 2005). W80 in NESS-2 helps orientate NE for efficient NE translocation to the deeper high affinity site NESS-1 (Fig. 6*B*). With NE in NESS-1, a salt bridge then forms between R81 and D473 (Fig. 6*C*), as observed in $LeuT_{Aa}$-Leu co-crystal (Krishnamurthy and Gouaux, 2012; Singh et al., 2007), facilitating a shift to the open-to-in conformation and forward transport of NE and two Na^+ ions (Fig. 6*D*) (Krishnamurthy and Gouaux, 2012). An extracellular Cl^- ion then likely participates in the final step in substrate transport that releases NE and Na^+ ions intracellularly from the open-to-in confirmation (Fig. 6*D*), before an intracellular Cl^- ion facilitates the structural reorganization of NET back to the substrate binding conformation (Erreger et al., 2008; Tavoulari et al., 2009). Since we have established that NESS-2 is above NESS-1, it is likely that NE must bind first at NESS-2 before it is translocated to the higher affinity NESS-1 and transported.

These studies of NET transport also provide insights into the structural features contributing to substrate selectivity. Our docking studies also show that the catecholbenzene, catecholamine and β-hydroxyl of NE form inter-molecular interactions with NET while the catecolhydroxyl does not, suggesting that catecholhydroxyl may not be essential for transport. This observation can explain why NET can transport both NE and DA (Buck and Amara, 1994; Carboni and Silvagni, 2004), which differ only by this catecolhydroxyl (Fig. 1B). In contrast,

Molecular Pharmacology Fast Forward. Published on August 8, 2012 as DOI: 10.1124/mol.112.080630
This article has not been copyedited and formatted. The final version may differ from this version.

DAT is incapable of transporting NE, suggesting that the size of the catechol tail is a key determinant of DAT monoamine substrate specificity.

In conclusion, we have used the $LeuT_{Aa}$-Leu crystal structure as a template to identify a second extracellular NE binding site named NESS-2, which is essential for efficient substrate transport by NET. Mutating 14 of the 15 residues identified from modelling produced effects on substrate transport and/or SNRI binding, confirming the predictive value of NET models built from $LeuT_{Aa}$ crystal structures. The residues identified here are mostly conserved across monoamine transporters, suggesting they likely have similar roles in related SLC6 transporters. The identification of new residues in NESS-2 that directly interact with substrate NE and/or NX may facilitate the development of new monoamine transporter inhibitors.

Molecular Pharmacology Fast Forward. Published on August 8, 2012 as DOI: 10.1124/mol.112.080630
This article has not been copyedited and formatted. The final version may differ from this version.

Acknowledgements

We thank Dr. Lotten Ragnarsson-McGrath for molecular biology advice and help constructing difficult mutations.

Authorship contribution

Participated in research design: Wang, Shaikh, Lewis

Conducted experiments: Wang, Shaikh, Ramu

Contributed new reagents or analytic tools: Lewis

Performed data analysis: Wang, Shaikh, Lewis

Wrote or contributed to the writing of the manuscript: Wang, Lewis

Molecular Pharmacology Fast Forward. Published on August 8, 2012 as DOI: 10.1124/mol.112.080630
This article has not been copyedited and formatted. The final version may differ from this version.

References

Amara SG and Sonders MS (1998) Neurotransmitter transporters as molecular targets for addictive drugs. *Drug Alcohol Depend* **51**(1-2): 87-96.

Andersen J, Kristensen AS, Bang-Andersen B and Stromgaard K (2009) Recent advances in the understanding of the interaction of antidepressant drugs with serotonin and norepinephrine transporters. *Chem Commun (Camb)*(25): 3677-3692.

Barker EL, Moore KR, Rakhshan F and Blakely RD (1999) Transmembrane domain I contributes to the permeation pathway for serotonin and ions in the serotonin transporter. *J Neurosci* **19**(12): 4705-4717.

Beuming T, Kniazeff J, Bergmann ML, Shi L, Gracia L, Raniszewska K, Newman AH, Javitch JA, Weinstein H, Gether U and Loland CJ (2008) The binding sites for cocaine and dopamine in the dopamine transporter overlap. *Nat Neurosci* **11**(7): 780-789.

Beuming T, Shi L, Javitch JA and Weinstein H (2006) A comprehensive structure-based alignment of prokaryotic and eukaryotic neurotransmitter/Na^+ symporters (NSS) aids in the use of the LeuT structure to probe NSS structure and function. *Molecular Pharmacology* **70**(5): 1630-1642.

Bowie JU, Luthy R and Eisenberg D (1991) A method to identify protein sequences that fold into a known three-dimensional structure. *Science* **253**(5016): 164-170.

Brust A, Palant E, Croker DE, Colless B, Drinkwater R, Patterson B, Schroeder CI, Wilson D, Nielsen CK, Smith MT, Alewood D, Alewood PF and Lewis RJ (2009) χ-Conopeptide pharmacophore development: Toward a novel class of norepinephrine transporter inhibitor (Xen2174) for pain. *J Med Chem* **52**(22): 6991-7002.

Buck KJ and Amara SG (1994) Chimeric dopamine-norepinephrine transporters delineate structural domains influencing selectivity for catecholamines and 1-methyl-4-phenylpyridinium. *Proc Natl Acad Sci U S A* **91**(26): 12584-12588.

Carboni E and Silvagni A (2004) Dopamine reuptake by norepinephrine neurons: exception or rule? *Crit Rev Neurobiol* **16**(1-2): 121-128.

Chen J, Lu G, Lin J, Davidson AL and Quiocho FA (2003) A tweezers-like motion of the ATP-binding cassette dimer in an ABC transport cycle. *Mol Cell* **12**(3): 651-661.

Chen NH, Reith ME and Quick MW (2004) Synaptic uptake and beyond: The sodium- and chloride-dependent neurotransmitter transporter family SLC6. *Pflugers Arch* **447**(5): 519-531.

Dougherty DD, Bonab AA, Spencer TJ, Rauch SL, Madras BK and Fischman AJ (1999) Dopamine transporter density in patients with attention deficit hyperactivity disorder. *Lancet* **354**(9196): 2132-2133.

Emsley P and Cowtan K (2004) Coot: Model-building tools for molecular graphics. *Acta Cryst* **D60**: 2126-2132.

Erreger K, Grewer C, Javitch JA and Galli A (2008) Currents in response to rapid concentration jumps of amphetamine uncover novel aspects of human dopamine transporter function. *J Neurosci* **28**(4): 976-989.

Fiser A and Sali A (2003) Modeller: generation and refinement of homology-based protein structure models. *Methods Enzymol* **374**: 461-491.

Forrest LR, Tang CL and Honig B (2006) On the accuracy of homology modeling and sequence alignment methods applied to membrane proteins. *Biophys J* **91**(2): 508-517.

Forrest LR, Tavoulari S, Zhang YW, Rudnick G and Honig B (2007) Identification of a chloride ion binding site in Na^+/Cl^- -dependent transporters. *Proc Natl Acad Sci U S A* **104**(31): 12761-12766.

Forrest LR, Zhang YW, Jacobs MT, Gesmonde J, Xie L, Honig BH and Rudnick G (2008) Mechanism for alternating access in neurotransmitter transporters. *Proc Natl Acad Sci U S A* **105**(30): 10338-10343.

Gunsteren WFv and Berendsen HJC (1990) Computer simulation of molecular dynamics: Methodology, applications, and perspectives in chemistry. *Angewandte Chemie International Edition in English* **29**(9): 992-1023.

Hahn MK, Robertson D and Blakely RD (2003) A mutation in the human norepinephrine transporter gene (SLC6A2) associated with orthostatic intolerance disrupts surface expression of mutant and wild-type transporters. *J Neurosci* **23**(11): 4470-4478.

Henry LK, Defelice LJ and Blakely RD (2006) Getting the message across: a recent transporter structure shows the way. *Neuron* **49**(6): 791-796.

Huang X and Zhan CG (2007) How dopamine transporter interacts with dopamine: insights from molecular modeling and simulation. *Biophys J* **93**(10): 3627-3639.

Indarte M, Madura JD and Surratt CK (2008) Dopamine transporter comparative molecular modeling and binding site prediction using the LeuT(Aa) leucine transporter as a template. *Proteins* **70**(3): 1033-1046.

Jacobs MT, Zhang YW, Campbell SD and Rudnick G (2007) Ibogaine, a noncompetitive inhibitor of serotonin transport, acts by stabilizing the cytoplasm-facing state of the transporter. *J Biol Chem* **282**(40): 29441-29447.

Jayanthi LD, Prasad PD, Ramamoorthy S, Mahesh VB, Leibach FH and Ganapathy V (1993) Sodium- and chloride-dependent, cocaine-sensitive, high-affinity binding of nisoxetine to the human placental norepinephrine transporter. *Biochemistry* **32**(45): 12178-12185.

Jeon B, Kim JM, Jeong JM, Kim KM, Chang YS, Lee DS and Lee MC (1998) Dopamine transporter imaging with [^{123}I]-β-CIT demonstrates presynaptic nigrostriatal dopaminergic damage in Wilson's disease. *J Neurol Neurosurg Psychiatry* **65**(1): 60-64.

Ju P, Aubrey KR and Vandenberg RJ (2004) Zn^{2+} inhibits glycine transport by glycine transporter subtype 1b. *J Biol Chem* **279**(22): 22983-22991.

Kelley LA and Sternberg MJ (2009) Protein structure prediction on the Web: A case study using the Phyre server. *Nat Protoc* **4**(3): 363-371.

Kim HJ, Im JH, Yang SO, Moon DH, Ryu JS, Bong JK, Nam KP, Cheon JH, Lee MC and Lee HK (1997) Imaging and quantitation of dopamine transporters with iodine^{123}-IPT in normal and Parkinson's disease subjects. *J Nucl Med* **38**(11): 1703-1711.

Klimek V, Stockmeier C, Overholser J, Meltzer HY, Kalka S, Dilley G and Ordway GA (1997) Reduced levels of norepinephrine transporters in the locus coeruleus in major depression. *J Neurosci* **17**(21): 8451-8458.

Krishnamurthy H and Gouaux E (2012) X-ray structures of LeuT in substrate-free outward-open and apo inward-open states. *Nature* **481**(7382): 469-474.

Krishnamurthy H, Piscitelli CL and Gouaux E (2009) Unlocking the molecular secrets of sodium-coupled transporters. *Nature* **459**(7245): 347-355.

Krogh A, Larsson B, von Heijne G and Sonnhammer EL (2001) Predicting transmembrane protein topology with a hidden Markov model: application to complete genomes. *J Mol Biol* **305**(3): 567-580.

Larkin MA, Blackshields G, Brown NP, Chenna R, McGettigan PA, McWilliam H, Valentin F, Wallace IM, Wilm A, Lopez R, Thompson JD, Gibson TJ and Higgins DG (2007) ClustalW and ClustalX version 2. *Bioinformatics* **23**(21): 2947-2948.

Laskowski RA, Watson JD and Thornton JM (2005) ProFunc: A server for predicting protein function from 3D structure. *Nucl Acids Res* **33**: W89-W93.

Masson J, Sagne C, Hamon M and El Mestikawy S (1999) Neurotransmitter transporters in the central nervous system. *Pharmacol Rev* **51**(3): 439-464.

Mitchell SM, Lee E, Garcia ML and Stephan MM (2004) Structure and function of extracellular loop 4 of the serotonin transporter as revealed by cysteine-scanning mutagenesis. *J Biol Chem* **279**(23): 24089-24099.

Nielsen CK, Lewis RJ, Alewood D, Drinkwater R, Palant E, Patterson M, Yaksh TL, McCumber D and Smith MT (2005) Anti-allodynic efficacy of the chi-conopeptide, Xen2174, in rats with neuropathic pain. *Pain* **118**(1-2): 112-124.

Norregaard L, Frederiksen D, Nielsen EO and Gether U (1998) Delineation of an endogenous zinc-binding site in the human dopamine transporter. *Embo J* **17**(15): 4266-4273.

Paczkowski FA, Sharpe IA, Dutertre S and Lewis RJ (2007) χ-Conotoxin and tricyclic antidepressant interactions at the norepinephrine transporter define a new transporter model. *Journal of Biological Chemistry* **282**(24): 17837-17844.

Piscitelli CL, Krishnamurthy H and Gouaux E (2010) Neurotransmitter/sodium symporter orthologue LeuT has a single high-affinity substrate site. *Nature* **468**(7327): 1129-1132.

Quick M, Shi L, Zehnpfennig B, Weinstein H and Javitch JA (2012) Experimental conditions can obscure the second high-affinity site in LeuT. *Nat Struct Mol Biol* **19**(2): 207-211.

Quick M, Winther AM, Shi L, Nissen P, Weinstein H and Javitch JA (2009) Binding of an octylglucoside detergent molecule in the second substrate (S2) site of LeuT establishes an inhibitor-bound conformation. *Proc Natl Acad Sci U S A* **106**(14): 5563-5568.

Ritchie DW and Kemp GJL (2000) Protein docking using spherical polar Fourier correlations. *Proteins-Structure Function and Genetics* **39**(2): 178-194.

Ritz MC, Lamb RJ, Goldberg SR and Kuhar MJ (1987) Cocaine receptors on dopamine transporters are related to self-administration of cocaine. *Science* **237**(4819): 1219-1223.

Rudnick G and Wall SC (1992) The molecular mechanism of "ecstasy" [3,4-methylenedioxy-methamphetamine (MDMA)]: Serotonin transporters are targets for MDMA-induced serotonin release. *Proc Natl Acad Sci U S A* **89**(5): 1817-1821.

Sharpe IA, Gehrmann J, Loughnan ML, Thomas L, Adams DA, Atkins A, Palant E, Craik DJ, Adams DJ, Alewood PF and Lewis RJ (2001) Two new classes of conopeptides inhibit the α_1-adrenoceptor and noradrenaline transporter. *Nat Neurosci* **4**(9): 902-907.

Shi L, Quick M, Zhao Y, Weinstein H and Javitch JA (2008) The mechanism of a neurotransmitter:sodium symporter--inward release of Na^+ and substrate is triggered by substrate in a second binding site. *Mol Cell* **30**(6): 667-677.

Singh SK, Piscitelli CL, Yamashita A and Gouaux E (2008) A competitive inhibitor traps LeuT in an open-to-out conformation. *Science* **322**(5908): 1655-1661.

Singh SK, Yamashita A and Gouaux E (2007) Antidepressant binding site in a bacterial homologue of neurotransmitter transporters. *Nature* **448**(7156): 952-956.

Sinning S, Musgaard M, Jensen M, Severinsen K, Celik L, Koldso H, Meyer T, Bols M, Jensen HH, Schiott B and Wiborg O (2010) Binding and orientation of tricyclic antidepressants within the central substrate site of the human serotonin transporter. *J Biol Chem* **285**(11): 8363-8374.

Smicun Y, Campbell SD, Chen MA, Gu H and Rudnick G (1999) The role of external loop regions in serotonin transport. Loop scanning mutagenesis of the serotonin transporter external domain. *J Biol Chem* **274**(51): 36058-36064.

Stephan MM, Chen MA, Penado KM and Rudnick G (1997) An extracellular loop region of the serotonin transporter may be involved in the translocation mechanism. *Biochemistry* **36**(6): 1322-1328.

Tang L, Bai L, Wang WH and Jiang T (2010) Crystal structure of the carnitine transporter and insights into the antiport mechanism. *Nat Struct Mol Biol* **17**(4): 492-496.

Tavoulari S, Forrest LR and Rudnick G (2009) Fluoxetine (Prozac) binding to serotonin transporter is modulated by chloride and conformational changes. *J Neurosci* **29**(30): 9635-9643.

Trott O and Olson AJ (2010) AutoDock Vina: Improving the speed and accuracy of docking with a new scoring function, efficient optimization, and multithreading. *J Comput Chem* **31**(2): 455-461.

Vriend G (1990) What If - a Molecular Modeling and Drug Design Program. *Journal of Molecular Graphics* **8**(1): 52-56.

Wang H, Elferich J and Gouaux E (2012) Structures of LeuT in bicelles define conformation and substrate binding in a membrane-like context. *Nat Struct Mol Biol* **19**(2): 212-219.

Wong DF, Harris JC, Naidu S, Yokoi F, Marenco S, Dannals RF, Ravert HT, Yaster M, Evans A, Rousset O, Bryan RN, Gjedde A, Kuhar MJ and Breese GR (1996) Dopamine transporters are markedly reduced in Lesch-Nyhan disease in vivo. *Proc Natl Acad Sci U S A* **93**(11): 5539-5543.

Yamashita A, Singh SK, Kawate T, Jin Y and Gouaux E (2005) Crystal structure of a bacterial homologue of Na^+/Cl^--dependent neurotransmitter transporters. *Nature* **437**(7056): 215-223.

Zhang YW and Rudnick G (2006) The cytoplasmic substrate permeation pathway of serotonin transporter. *J Biol Chem* **281**(47): 36213-36220.

Zhao Y, Terry DS, Shi L, Quick M, Weinstein H, Blanchard SC and Javitch JA (2011) Substrate-modulated gating dynamics in a Na^+-coupled neurotransmitter transporter homologue. *Nature* **474**(7349): 109-113.

Zhou Z, Zhen J, Karpowich NK, Goetz RM, Law CJ, Reith ME and Wang DN (2007) LeuT-desipramine structure reveals how antidepressants block neurotransmitter reuptake. *Science* **317**(5843): 1390-1393.

Zhou Z, Zhen J, Karpowich NK, Law CJ, Reith ME and Wang DN (2009) Antidepressant specificity of serotonin transporter suggested by three LeuT-SSRI structures. *Nat Struct Mol Biol* **16**(6): 652-657.

Zomot E, Bendahan A, Quick M, Zhao Y, Javitch JA and Kanner BI (2007) Mechanism of chloride interaction with neurotransmitter:sodium symporters. *Nature* **449**(7163): 726-730.

Zomot E and Kanner BI (2003) The interaction of the gamma-aminobutyric acid transporter GAT-1 with the neurotransmitter is selectively impaired by sulfhydryl modification of a conformationally sensitive cysteine residue engineered into extracellular loop IV. *J Biol Chem* **278**(44): 42950-42958.

Molecular Pharmacology Fast Forward. Published on August 8, 2012 as DOI: 10.1124/mol.112.080630
This article has not been copyedited and formatted. The final version may differ from this version.

Footnotes:

C-I.A. Wang and N.H. Shaikh, contributed equally to the work. This research was supported by an Australian Research Council Discovery Grant [DP120101992] and a National Health and Medical Research Council Program grant [569927] to RJL.

Molecular Pharmacology Fast Forward. Published on August 8, 2012 as DOI: 10.1124/mol.112.080630
This article has not been copyedited and formatted. The final version may differ from this version.

Legend to Figures

Fig. 1. Homology model of human NET viewed from the side (*A*, left) or from an extracellular view (*A*, right). The final docking results of substrate norepinephrine (green) and competitive inhibitor nisoxetine (orange) to the occluded conformation are presented in stick form at NESS-2. The second substrate binding site (NESS-1), which is equivalent to Leu binding site found in $LeuT_{Aa}$(Yamashita et al., 2005), is indicated with the top 10 energetically favourable docking solutions for NE shown in black (*A*, left). The specific inter-molecular interactions observed for the binding of norepinephrine at NESS-2 (*B*) and nisoxetine (*C*) reveal that both binding sites partially overlap and are dominated by hydrophobic interactions. The catecolhydroxyl, the only difference between norepinephrine and dopamine, is indicated by the blue circle (*B*, left). For clarity, the 3D structures are presented in 50% transparency.

Fig. 2. Residues (purple) predicted to contribute structurally to substrate transport and inhibitor binding in NET. These residues stabilize the integrity of NESS-2 by forming extensive hydrophobic network with residues (green) from different TMHs. The overall positions are shown in the left (side view) and middle (top view) panels, with detailed intra-molecular interactions presented in the right panel. The 3D structures are presented in 50% transparency.

Fig. 3 Immunodetection (*A*) and single-point normalized NX binding (100% = 1.7 nmol/mg total protein) and NE uptake (100% = 4.2 x 10^{-14} mol/min/cell) (*B*) for NET and mutants. The immunodetection indicates that alanine substitution for D75 and L76 abolishes the transporter expression, and S419A mutant causes misfolding of NET transporter. The effect of each mutation on and NX binding (open bar) and NE uptake (closed bar) are presented as means ± standard error of at least three independent experiments, each performed in triplicate.

Molecular Pharmacology Fast Forward. Published on August 8, 2012 as DOI: 10.1124/mol.112.080630
This article has not been copyedited and formatted. The final version may differ from this version.

Fig. 4. NE uptake (*A*) and NX binding saturation (*C*) and displacement assays (*B,D*) for wild-type NET (WT) and mutants. All mutants were subjected for uptake and binding saturation and displacement assays. Mutants that showed no detectable uptake (up to 5 μM (^{3}H)NE) or binding (50 nM (^{3}H)NX) activity are not shown for clarity. Mutants that significant affected NE uptake or/and NX binding are indicated with an asterix (*). Each value represents the mean ± standard error of at least three independent experiments, each performed in triplicate. Additional kinetics data are summarised in Table 2.

Fig. 5. Docking simulation of NE and NX to the W80A-NET homology model. The identified NE and NX in NET are shown in green half transparent surface and orange dot mesh, respectively. The top 10 energetically favourable NE (blue) and NX (purple) docking solutions to W80A-NET presented in stick in (*A*) and (*B*), respectively. Position of residue W80A is presented in red stick. (*A*) The docking showed that the initial NE binding site (green) is no longer energetically favourable for binding due to the loss of the hydrophobic interaction provided by W80, and that NE binding site is shifted to completely overlap with NX binding site, in agreement with our NX displacement assays (Fig 5). (*B*) In contrast, NX docked in the same binding site with slightly different orientation, which may explain the ~ 5-fold improvement in binding affinity (K_D).

Fig. 6. A schematic of the proposed substrate transport mechanism for NET. In this model, NE (green) first transitions from a low affinity site NESS-2 (A), to a deeper high affinity site NESS-1 (B). With NE in NESS-1, a salt bridge forms between R81 and D473 and an extracellular Cl^- ion binds (orange sphere), facilitating the forward transport of NE and two Na^+ ions (yellow) (E). To complete the cycle, an intracellular Cl^- ion binds to NET and facilitates a conformational change(s) from the transporting to the substrate binding conformation (A). For clarity, only the core TMHs are shown.

Molecular Pharmacology Fast Forward. Published on August 8, 2012 as DOI: 10.1124/mol.112.080630
This article has not been copyedited and formatted. The final version may differ from this version.

Table 1. The assessment of structural relationship between NET model and $LeuT_{Aa}$ crystal structure. The relationship of protein sequence identity and the expected model accuracy based on the backbone RMSD comparison is derived from Forrest et al. (2006) are shown overall and for NESS-1 and NESS-2.

	Residues	Number of residues	Identity (%)	Expected RMSD (Å) to $LeuT_{Aa}$	R.M.S.D (Å) to $LeuT_{Aa}$
Overall	56-582 (5-515)	527/511	27	≥2.5	1.394
NESS-1 vs S1	72-78 (21-27) 156-159 (104-107) 317-323 (253-259) 419-423 (355-359)	23/23	47.8	<2	0.426
NESS-2 vs S2	79-85 (28-34) 160-164 (109-113) 308-316 (244-252) 467-473 (398-404)	28/28	42.8	<2	0.482

Table 2. Norepinephrine (NE) and nisoxetine (NX) uptake and affinity at hNET and mutants.

	Mutation Position	(^{3}H)NX K_D (nM)	(^{3}H)NE K_M (μM)	NE IC_{50} (μM)$^{\#}$	NX IC_{50} (nM)$^{\#}$	(^{3}H)NX B_{MAX} (%)	(^{3}H)NE V_{MAX} (%)
hNET		4.1± 0.5	1.03± 0.02	59 ± 3.4	3.4 ± 0.7	100	100
D75A	Loop1a-1b	low NET expression (~ 3% of hNET)					
L76A	TMH1b	no detectable NET expression					
W80A	TMH1b	0.8 ± 0.3*	NDR	32 ± 1.7	ND	64 ± 7.2	NDR
R81A	TMH1b	NDR		not determined			
R81D	TMH1b						
R81Q	TMH1b	1.98 ± 0.6	NDR	97 ± 18.2	ND	21 ± 5 *	NDR
Y84A	TMH1b	19.6± 2.5*	0.57 ± 0.6	78 ± 7.6	38 ± 10*	112.7 ± 16.2	81± 16
L160A	TMH3	2.7 ± 0.5	1.14 ± 0.1	89 ± 6.8	6.7 ± 2.5	45 ± 7	92.6 ± 28.7
F164A	TMH3	3.9 ± 1.23	0.2±0.01*	70 ± 7.4	6.6 ± 2	29 ± 0.9*	28.5 ± 11*
W308A	TMH6a	NDR		not determined			
Q314A	TMH6a	0.91 ±0.1*	NDR	43 ± 17.4	ND	69.1 ± 9.65	NDR
F316A	TMH6a	9.3 ± 0.4	1.20 ±0.26	47 ± 17	ND	95.2 ± 1	3.44 ± 0.02*
F317A	TMH6a	NDR		not determined			
F388A	EL4						
S419A	TMH8	misfolded NET					
Y467A	TMH10	NDR		not determined			
Y467F	TMH10	2.56 ± 0.2	0.61 ±0.13	211 ± 30*	ND	16.7 ± 4.9*	10.9 ± 4.9*
D473A	TMH10	0.95 ±0.3*	NDR	371 ± 82*	ND	95 ± 17.6	NDR
D473R	TMH10	0.98 ±0.4*	NDR	93 ± 8.8	ND	35.6 ± 5.8	NDR
R81D/D473R	TMH1b/10	0.87 ±0.3*	NDR	115 ± 12.2	ND	26.6 ± 2.9*	NDR
R81Q/Q314R	TMH1b/6a	NDR		not determined			
R81A/Q314A	TMH1b/6a						

Data are means ± SEM of three or four independent experiments separately analyzed in Prism 5. B_{MAX} and V_{MAX} are per 20 μg of total cellular protein and ~50,000 cells, respectively.

*Statistically significant compared to hNET wild type (one-way ANOVA, $p<0.05$).

[#]NE IC_{50} determined from displacement of (^{3}H)NX, and NX IC_{50} determined from inhibition of (^{3}H)NE uptake.

NDR, no detectable response for either specific NX binding up to 200 nM (^{3}H)NX, or specific NE uptake up to 5 μM (^{3}H)NE (3-5 separate experiments).

ND, not determined.

Figure 1 Molecular Pharmacology Fast Forward. Published on August 8, 2012 as DOI: 10.1124/mol.112.080630
This article has not been copyedited and formatted. The final version may differ from this version.

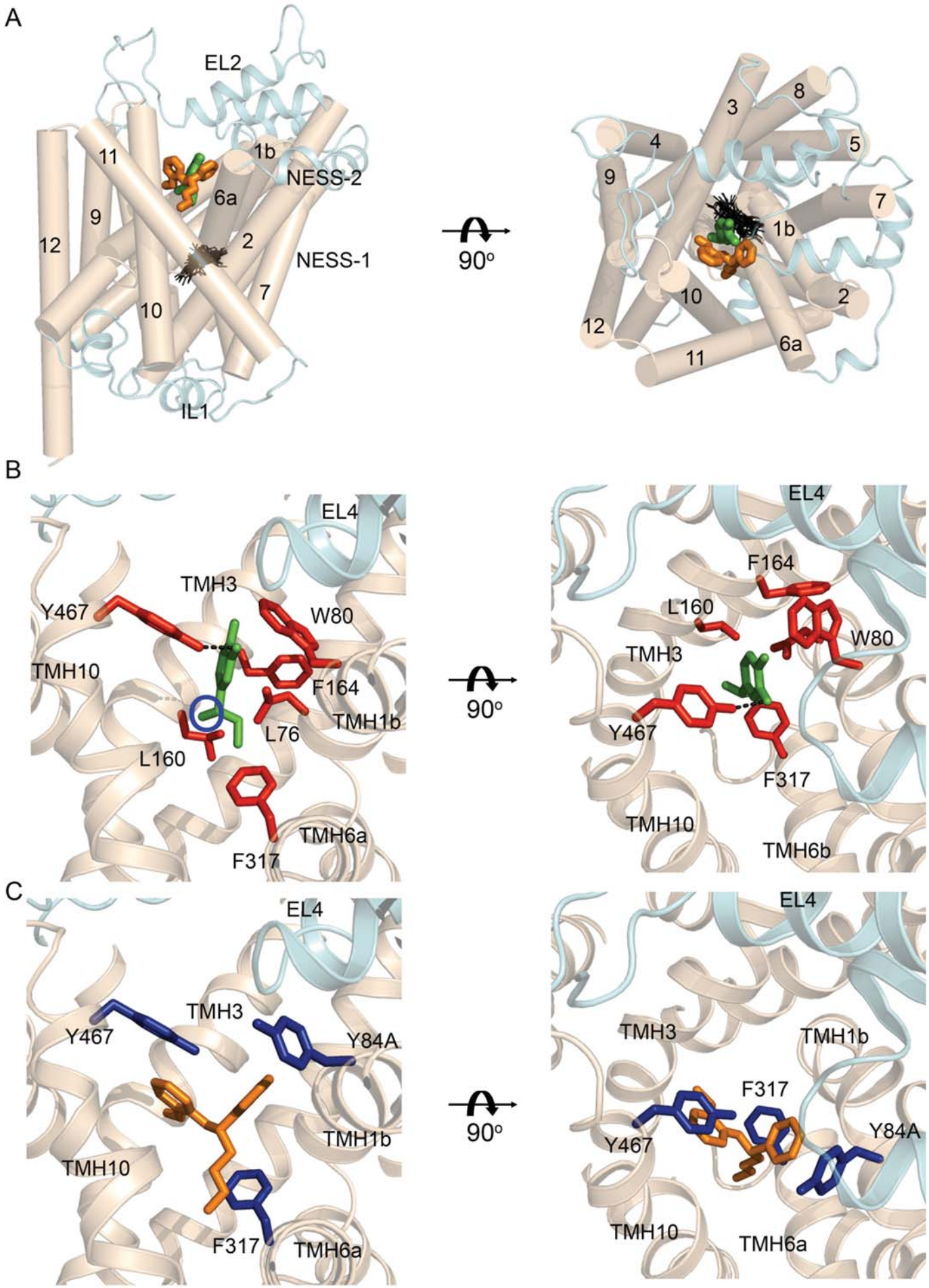

Figure 2 Molecular Pharmacology Fast Forward. Published on August 8, 2012 as DOI: 10.1124/mol.112.080630
This article has not been copyedited and formatted. The final version may differ from this version.

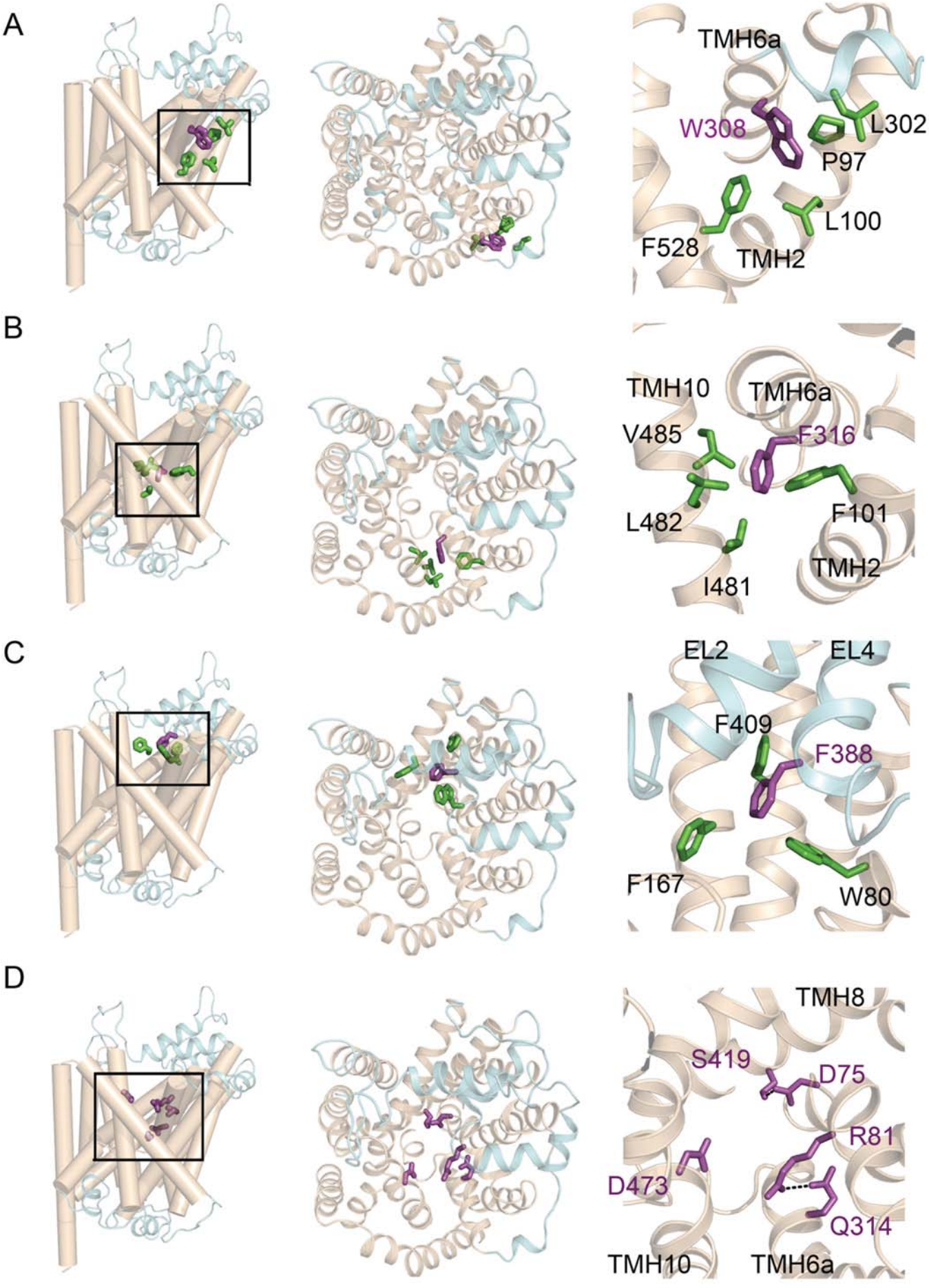

Molecular Pharmacology Fast Forward. Published on August 8, 2012 as DOI: 10.1124/mol.112.080630
This article has not been copyedited and formatted. The final version may differ from this version.

Figure 3

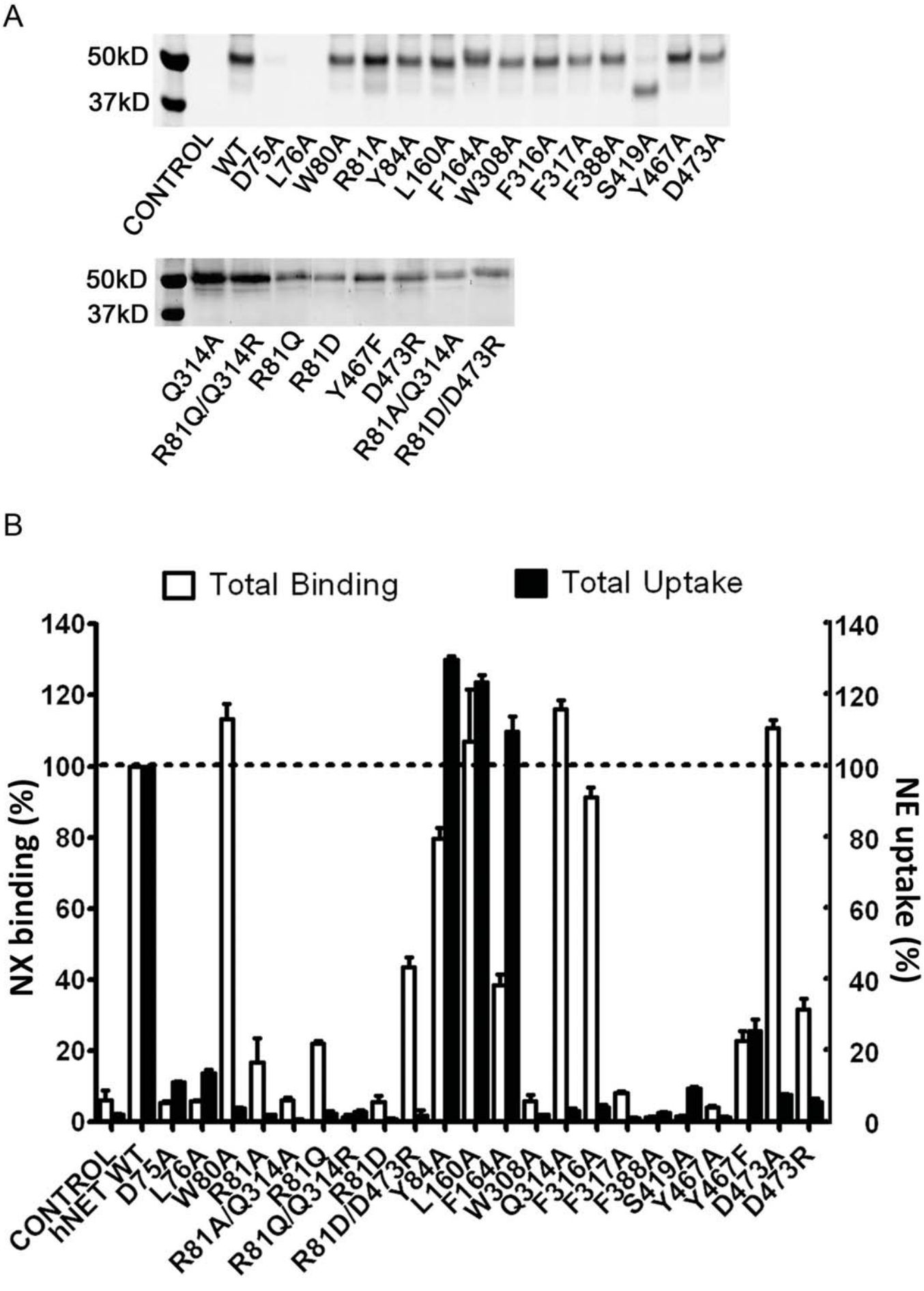

Molecular Pharmacology Fast Forward. Published on August 8, 2012 as DOI: 10.1124/mol.112.080630
This article has not been copyedited and formatted. The final version may differ from this version.

Figure 4

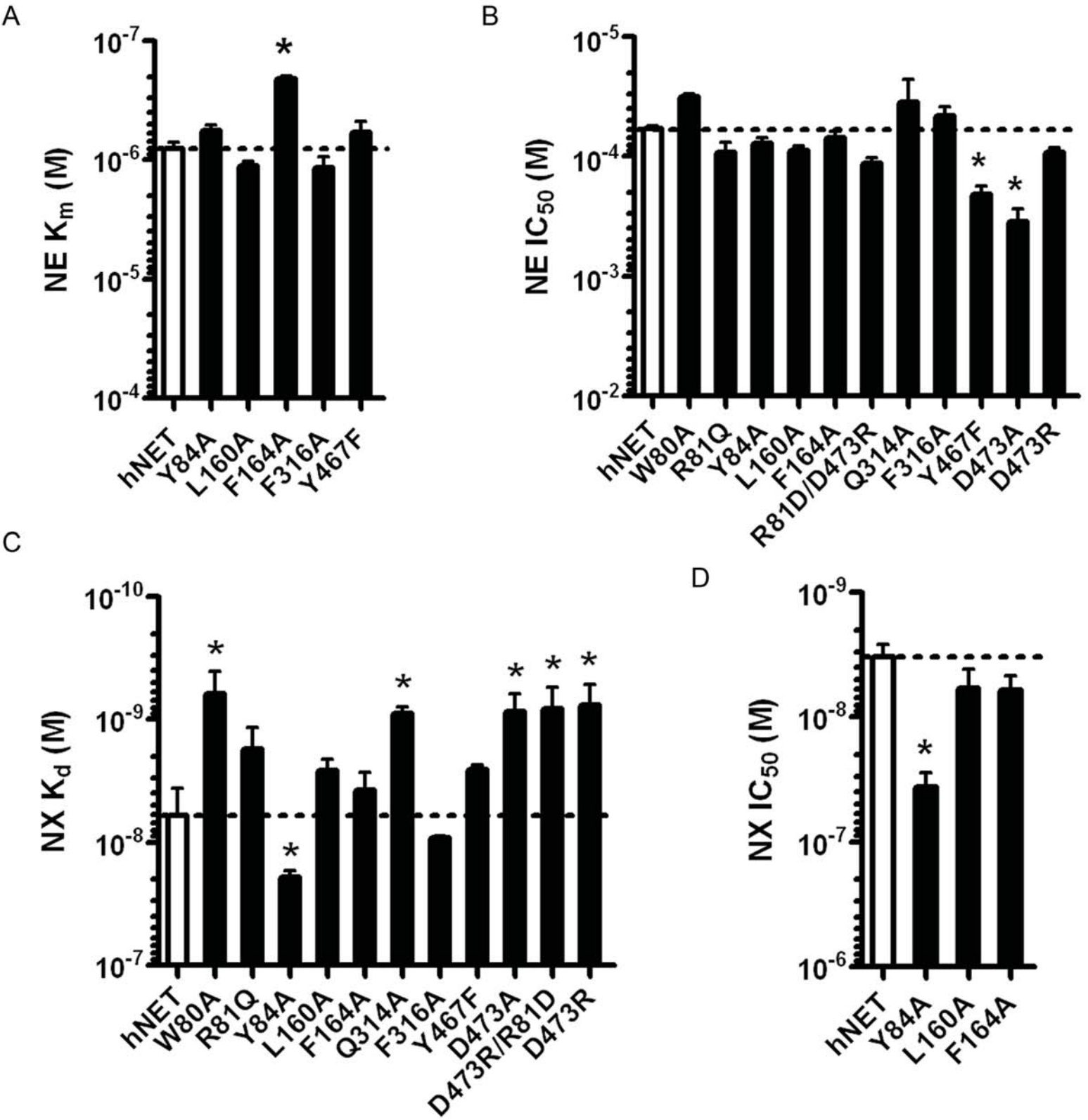

Figure 5

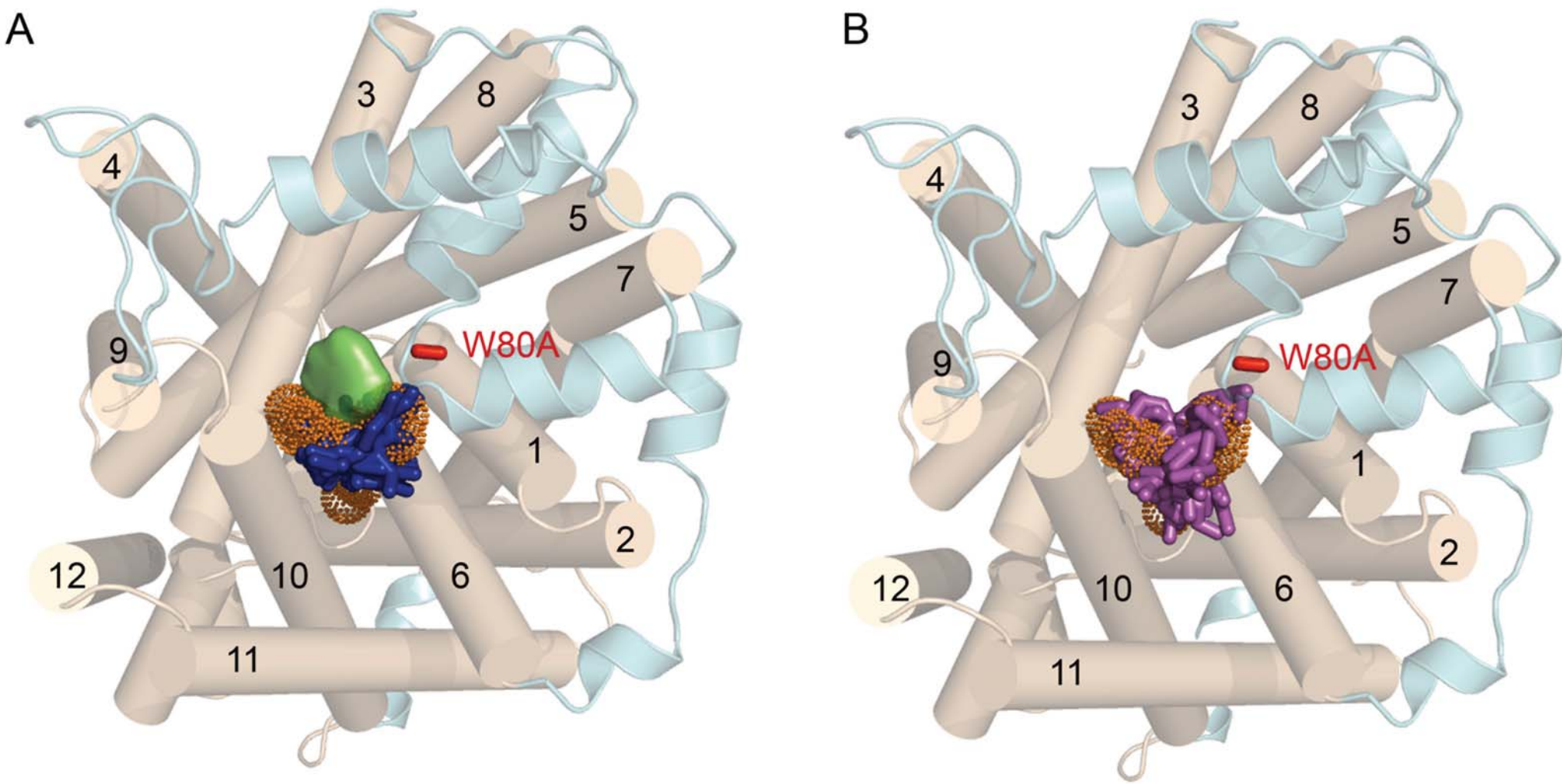

Molecular Pharmacology Fast Forward. Published on August 8, 2012 as DOI: 10.1124/mol.112.080630
This article has not been copyedited and formatted. The final version may differ from this version.

Figure 6